Intercontinental transport of pollution manifested in the variability and seasonal trend of springtime O_3 at northern mid and high latitudes

Yuhang Wang,[1] Changsub Shim,[1] Nicola Blake,[2] Donald Blake,[2] Yunsoo Choi,[1] Brian Ridley,[3] Jack Dibb,[4] Anthony Wimmers,[5] Jennie Moody,[5] Frank Flocke,[3] Andrew Weinheimer,[3] Robert Talbot,[4] and Elliot Atlas[3]

J. Geophy. Res.
In press, July 2003

Corresponding author: Yuhang Wang, School of Earth and Atmospheric Sciences, Georgia Institute of Technology, Atlanta, GA 30332-0340. (Email: ywang@eas.gatech.edu)

---

[1]School of Earth and Atmospheric Sciences, Georgia Institute of Technology, Atlanta, Georgia.
[2]Department of Chemistry, University of California at Irvine, Irvine, California.
[3]National Center for Atmospheric Research, Boulder, Colorado.
[4]Institute for the Study of Earth, Oceans, and Space, University of New Hampshire, Durham, New Hampshire.
[5]Department of Environmental Sciences, University of Virginia, Charlottesville, Virginia.

Abstract. Observations (0-8 km) from the Tropospheric Ozone Production about the Spring Equinox (TOPSE) experiment are analyzed to examine air masses contributing to the observed variability of springtime O_3 and its seasonal increase at 40-85° N over North America. Factor analysis using the PMF and PCA methods is applied to the dataset with 14 chemical tracers (O_3, NO_y, PAN, CO, CH_4, C_2H_2, C_3H_8, CH_3Cl, CH_3Br, C_2Cl_4, CFC-11, HCFC-141B, Halon-1211, and ^7Be) and 1 dynamic tracer (potential temperature). Our analysis results are biased by the measurements at 5-8 km (70% of the data) due to the availability of ^7Be measurements. The identified tracer characteristics for 7 factors are generally consistent with the geographical origins derived from their 10-day backtrajectories. Stratospherically influenced air accounts for 14 ppbv (35-40%) of the observed O_3 variability for data with O_3 concentrations < 100 ppbv at mid and high latitudes. It accounts for about 2.5 ppbv/month (40%) of the seasonal O_3 trend at mid latitudes but only 0.8 ppbv/month (<20%) at high latitudes, likely reflecting more vigorous mid-latitude dynamical systems in spring. At mid latitudes, reactive nitrogen rich air masses transported through Asia are much more significant (11 ppbv in variability and 3.5 ppbv/month in trend) than other tropospheric contributors. At high latitudes, the O_3 variability is significantly influenced by air masses transported from lower latitudes (11 ppbv), which are poor in reactive nitrogen. The O_3 trend, in contrast, is largely defined by air masses rich in reactive nitrogen transported through Asia and Europe across the Pacific or the Arctic (3 ppbv/month). The influence from the stratospheric source is more apparent at 6-8 km while the effect of O_3 production and transport within the troposphere is more apparent at lower altitudes. The overall effect of tropospheric photochemical production, through long-range transport, on the observed O_3

variability and its seasonal trend is more important at high latitudes relative to more photochemically active mid latitudes.

1. Introduction

Ozone in the troposphere is either produced photochemically within the troposphere or transported from the stratosphere. Its concentrations have important environmental ramifications. At high concentrations near the surface, it is hazardous to humans and plants. It is important for maintaining the oxidation capacity of the atmosphere through its photolysis to $O(^1D)$, which reacts with H_2O to produce OH radicals. Furthermore, it is an effective greenhouse gas.

An interesting feature of tropospheric O_3 is the observed springtime increase at northern mid and high latitudes. Ozone concentrations at northern mid and high latitudes tend to peak in late spring (April and May) in the lower troposphere and in early/mid summer (May-July) in the middle troposphere [e.g., Logan, 1985]. Levy et al. [1985] was able to simulate the springtime increase in a global 3-D model, which did not incorporate tropospheric chemistry. Penkett and Brice [1986] and Liu et al. [1987] suggested that the increase is driven by photochemical production in the troposphere. However, subsequent analysis work based on the observed correlation between O_3 and ^7Be tends to emphasize the effect of the stratospheric input [e.g., Oltmans and Levy, 1992; Dibb et al., 1994].

More recent analyses using photochemical models tend to emphasize the effect of tropospheric photochemical production. Photochemical box model calculations based on the measurements during the Free Tropospheric Experiment (FREETEX'96 and 98) in the Swiss Alps (at an altitude of 3.6 km) [Carpenter, 2000; Zanis et al., 2000] and aircraft observations during the Tropospheric Ozone Production about the Spring Equinox (TOPSE) experiment [e.g., Cantrell et al., 2003; Wang et al., 2003] showed that tropospheric O_3 production at mid latitudes are large enough to explain the observed

springtime O_3 increase at northern mid latitudes, although in situ O_3 production is ineffective at high latitudes [Wang et al., 2003]. Using global 3-D chemistry and transport models, Wang et al. [1998] showed that both factors contributed to the simulated springtime O_3 maximum at low altitudes (0-2 km) with one peaking in early spring and the other peaking in early summer, while Yienger et al. [1999] emphasized the effect of net O_3 chemical production at mid latitudes. Li et al. [2002] further suggested that the apparent correlation between surface observations of O_3 and ^7Be in Bermuda merely reflects the subsidence of O_3 produced in the middle troposphere not transported from the stratosphere.

Applying global 3-D chemistry and transport models, a number of recent studies have investigated the effects of intercontinental transport on tropospheric O_3 concentrations from Asia to North America [e.g., Bey et al., 2001; Berntsen et al., 1999; Jacob et al., 1999; Jaffe et al., 1999]. The effect of trans-Pacific transport is particularly large in spring [e.g., Wang et al., 1998; Jacob et al., 1999; Mauzerall et al., 2000; Wild and Akimoto, 2001; Tanimoto et al., 2002].

We analyze here aircraft springtime observations from TOPSE (February-May, 2000) [Atlas et al., 1993]. Thirty eight science flights of the C-130 aircraft were conducted in 7 deployments (1-2 weeks apart), covering a latitude range of 40-85° N (Colorado to north of Thule, Greenland) and an altitude range from the surface up to 8 km. A comprehensive suite of chemical species related to the tropospheric chemistry of O_3, HO_x ($OH+HO_2$), and NO_x ($NO+NO_2$) were measured.

This dataset is the largest available that extends over broad latitude and altitude ranges on a seasonal time scale in spring. We will attempt to address in this work the

effects on tropospheric O_3 variability and trend by intercontinental transport of O_3 and its precursors from different tropospheric regions and by transport of O_3 from the stratosphere on the basis of TOPSE observations. We will apply a multivariate analysis technique in this work. As illustrated by Li et al. [2002] and Browell et al. [2003], considering multiple correlations among O_3 and other species is critical.

2. Methodology

In this work, we analyze the covariant factors of 14 relatively long-lived chemical tracers and potential temperature. Our hypothesis is that air masses with varying contributions to the observed O_3 variability and trend can be differentiated on the basis of the covariance of their chemical compositions and that their geographical origins can be evaluated using backtrajectory calculations.

To examine the tracer profiles of various air masses, we applied two analytical methods, Principal Component Analysis (PCA) and the Positive Matrix Factorization (PMF) method. Covariance among the tracers is analyzed in these methods to define key components or factors that explain the variability of the data set. The PCA method [Press et al., 1992] with varimax rotation [Kaiser, 1958] yields comparable results as those by PMF. We find, however, that the PMF results are clearer for physical interpretations and for the separation of air masses than those by PCA because the latter lumps positively correlated tracers with negatively correlated tracers. Furthermore, the PMF results are more robust with respect to rotation. Only PMF results are discussed hereafter.

Our results cannot be directly compared to model estimated fractional contributions to tropospheric O_3 from different sources. Any correlation-based methods including the ones used here can only be used to examine the variability in the

observations. However, the results from variability analysis as those to be presented here are valuable because (1) they are based on the observations and are not affected by model imperfections and (2) the resulting concentration variability is often a key parameter with regard to potential environmental impact of a given factor. In order to fully reconcile our data analysis with those from the 3-D chemistry and transport models, we will need to conduct detailed simulations with the same species and equivalent spatial and temporal resolutions as in the observations. That is beyond the scope of this work. It is also useful to note that the validity of the linear covariance assumption of PMF, PCA, and other similar analysis techniques is tested on whether the resulting factors or principal components can be physically explained. These mathematical techniques evaluate only the "likelihood" of a given setup of factors or principal components; the results may be non-physical. We choose the solution that entails the best physical explanation.

The profiles of covariant elements (factors) are identified through matrix decomposition in the PMF method [Paatero, 1997]. The data matrix X of m measurements by n tracers can be decomposed for p factors as,

$$X = GF + E \tag{1}$$

Or

$$x_{ij} = \sum_{k=1}^{p} g_{ik} f_{kj} + e_{ij} \tag{2}$$

$$i = 1, \ldots, m; \; j = 1, \ldots, n; \; k = 1, \ldots, p$$

where the m by p matrix G is the factor score, the p by n matrix F is the tracer profile, and the m by n matrix E is the error. In our analysis we use explained variation ($EV_{kj} = \sum_{i=1}^{m} \left| g_{ik} f_{kj} \right| / (\sum_{i=1}^{m} (\sum_{k=1}^{p} \left| g_{ik} f_{kj} \right| + \left| e_{ij} \right|))$) to define the contributions from each factor [Lee

et al., 1999]. Necessary matrix rotation is determined [Paatero et al., 2002]; we find that for this dataset the PMF results are not as sensitive to rotation as those with PCA. The PMF method has been used previously to identify sources of aerosols and trace gases [Polissar et al., 1998; Paterson et al., 1999; Ramadan et al., 2000].

Among the available measurements during TOPSE, we chose 14 chemical tracers and one dynamic tracer. They are among the longer-lived tracers in the TOPSE measurements. The tracers (other than O_3) must also have unique source or concentration distributions, so they could be used to identify the origins of air masses. The chemical tracers chosen for the analysis are O_3, total reactive nitrogen (NO_y), peroxyacetylnitrate (PAN), CO, CH_4, C_2H_2, C_3H_8, CH_3Cl, CH_3Br, C_2Cl_4, CFC-11 (CCl_3F), HCFC-141B (CH_3CCl_2F), Halon-1211 ($CBrClF_2$), and ^7Be. Total reactive nitrogen is a good tracer of air masses that intercepted large tropospheric NO_x emissions or stratospheric air. PAN is a byproduct of NO_x oxidation and is a good tracer for tropospheric reactive nitrogen. High concentrations of PAN often indicate occurrences of tropospheric O_3 production in the past and therefore tend to correlate with high O_3 concentrations in pollution plumes. Carbon monoxide and C_2H_2 are good tracers for combustion and C_3H_8 is a good liquefied gas tracer. Methane has many sources, some of which are collocated with industrial pollution sources. Methyl chloride and CH_3Br are thought to have substantial sources from the ocean and biomass burning. Tropical terrestrial biosphere is likely a major CH_3Cl source region [Yokouchi et al., 2000; Lee-Taylor et al., 2001]. Tetrachloroethene is mainly a tracer for industrial activities. The production of CFC-11 and Halon-1211 was phased out in the developed countries at the end of 1995 and will be phased out in developing countries by 2010. HCFC-141b is a replacement for CFCs. Beryllium-7 is

produced by cosmic rays and is generally used as a tracer for stratospheric air [e.g., Dibb et al., 2003]. The other tracer we use in the analysis is potential temperature (θ), which is conserved during adiabatic processes. Potential vorticity is another useful dynamic tracer. It needs to be computed on the basis of θ and model simulated horizontal winds; the resulting temporal and spatial resolutions of this variable are much lower than the in situ measurements.

The observed values of each variable are linearly scaled to a dimensionless range of 0 to 1 and a small constant error estimate is assigned for equal weighting. In our analysis, no tracer should be weighted more than the other because they represent different processes. Our goal is not to define the best correlation between two specific tracers but rather to define the best tracer characteristics of air masses on the basis of the variability of all the tracers. Only data above the detection limits are used. By evaluating the error matrix E [Paatero, 1997; Lee et al., 1999; Paatero et al., 2002], we found that a range of 6-10 factors are appropriate for our data sets. We chose to use 7 factors, which separate air mass tracer profiles well.

The 10-day kinematic backtrajectories used in this work are calculated using the HYbrid Single-Particle Lagrangian Integrated Trajectory (HYSPLIT) model [Draxler and Hess, 1998]. The meteorological data are taken from the 'FNL' archive produced in the NOAA Air Resources Laboratory. The 6-hour archive is computed using a global data assimilation system [Kanamitsu, 1989]. This type of trajectory calculation is generally accurate for identifying large geographical features of air mass origins [Stohl, 1998]. The choice of 10 days for the backtrajectory calculation is somewhat arbitrary; it is long enough to separate local influence from long-range transport [Pocharnart et al., 2001].

3. Results and discussion

The photochemical environment is quite different from mid to high latitudes due in part to varying solar isolation [Wang et al., 2003]. Consequently, our analysis is conducted separately for these two regions. The size of our dataset is limited mostly by the availability of ^{7}Be data to 137 coincident measurements of all species at mid latitudes (40-60° N) and 193 coincident measurements at high latitudes (60-85° N). Including missing ^{7}Be data by assigning large uncertainties [Polissar et al., 1998] led to an underweight of the ^{7}Be data, resulting in a poor O_3-^{7}Be correlation and a large fraction of unexplained ^{7}Be variability. As demonstrated by Li et al. [2002] and Dibb et al. [2003], faithfully capturing the O_3-^{7}Be correlation is critical to resolve the contributions by various O_3 sources. Hence no missing ^{7}Be data were included. Ozone concentrations in this subset show similar probability distributions (binned by 10 ppbv) as the dataset with all measured O_3. The altitude distribution is shifted to higher altitude. The fraction of data above 5 km increases from 50% of all O_3 data to 70%. The seasonal O_3 trend of the subset is in agreement with that of all O_3 measurements above 5 km. Our results are therefore biased towards the middle and upper troposphere. The analysis results are about the same when measurements below 3 km are excluded.

In order to establish the correlation between the stratospheric O_3 and ^{7}Be, we have included in our analysis data points with O_3 concentrations > 100 ppbv (5% of the dataset), which are generally associated with the lower stratospheric air. To minimize the effects of these lower stratospheric data, our results are shown for data with O_3 concentrations < 100 ppbv. Relative to the results with all the data included, the effects of limited O_3 range are only apparent for O_3 and ^{7}Be and the estimated stratospheric contribution to O_3 variability is reduced. The EV percentages of O_3 in the factors

(defined in section 2) change by < 5%. The largest changes are seen in the explained variations of O_3 and ^7Be in the ^7Be factor, which decrease by 6 ppbv and 100-150 fCi/SCM, respectively.

3.1 Mid latitudes

The EV profiles of the 7 factors and the total EV explained by the analysis for data with O_3 concentrations < 100 ppbv are shown in Figure 1. The factors are named after their major components. Our analysis captures 80-95% of the observed variation of each tracer. The absolute tracer variation explained by each factor is shown in Figure 2. Five factors are mostly related to the sources and transport of CO, hydrocarbons, and halocarbons. The seasonal decrease of CO and hydrocarbons [e.g., Blake et al., 2003] is captured by the hydrocarbon factor.

Among the 7 factors, only ^7Be and NO_y-PAN factors account for >5% of the observed variability of O_3. The tracer profile of the ^7Be factor is consistent with a stratospheric origin. Potential temperature and HNO_3 concentrations in the stratosphere are much higher than those in the troposphere. The latter is reflected in the signal of NO_y, which encompasses all reactive nitrogen species. The factor shows no signal of PAN, which is produced in the troposphere. On the basis of our preliminary global 3-D simulations of CH_3Cl, we believe that the signal of CH_3Cl in the ^7Be factor likely reflects a general latitudinal gradient increasing towards tropics and the isentropic mixing of tropical and stratospheric air. The variability of CH_3Cl and CH_3Br explained by this factor is relatively small at 4 pptv and 0.15 pptv, respectively.

We estimate that stratospherically influenced air accounts for about 40% (14 ppbv) of the observed O_3 variation (Figs. 1 and 2). An uncertainty in our analysis comes from

the significant ^{7}Be source in the upper troposphere [e.g., Liu et al, 2001; Allen et al., 2003]. However, ^{7}Be concentrations are much lower in the upper tropospheric than the stratosphere due to the large difference of air residence time. Allen et al. [2003] showed that the variability due to ^{7}Be produced in the stratosphere is much larger than that produced in the troposphere. It is a good tracer for the stratospheric air in the context of the observed variability during TOPSE [D. Allen, personal communication, 2002]. Furthermore, an upper tropospheric ^{7}Be source does not necessarily imply that it will bias our results to favor the effect of stratospheric O_3. On the contrary, it would lead to an underestimate of the effect of stratospheric O_3 if the enhancement in ^{7}Be is not accompanied by comparable enhancement in O_3 concentrations. It is in fact the case for TOPSE; the $\Delta O_3 / \Delta^{7}\mathrm{Be}$ ratio from a least-squares fit for data above 6 km is about half of that for those below 6 km. The resulting bias for our analysis is small because the least-squares fitted $\Delta O_3 / \Delta^{7}\mathrm{Be}$ ratio for the whole dataset is about the same as that for data above 6 km.

The Bermuda O_3-^{7}Be correlation analysis by Li et al. [2002] appears to show results that differ from our work for TOPSE. The data they used were collected near the surface during March-May, 1996 in Bermuda (32° N). The season is similar but the latitude and sampling altitude are different. During TOPSE, ^{7}Be concentrations up to 4000 fCi/SCM were observed while the Bermuda site measurements are < 250 fCi/SCM. A least-squares fit of TOPSE mid-latitude observations yields a slope of 0.04 ppbv/fCi/SCM. The correlation coefficient is 0.8, indicating that the variance of ^{7}Be explains about 65% of the O_3 variance. The variability ratio of O_3 to ^{7}Be in the ^{7}Be factor shows a similar value, 0.045 ppbv/fCi/SCM (Fig. 2). In comparison, Li et al. [2002]

showed a much larger slope of 0.45 ppbv/fCi/SCM; the correlation coefficient is very low, at only 0.36. The much higher O_3-^{7}Be slope at Bermuda indicates that transport from the stratosphere is not the major source of O_3 variability at Bermuda. If we simply scale the $\Delta O_3 / \Delta^7 Be$ obtained from the PMF analysis to the maximum variability of ^{7}Be at Bermuda (about 160 fCi/SCM), we would estimate a maximum stratospheric contribution of 7 ppbv to the observed O_3 variability at Bermuda during March-May, 1996. Furthermore, if we assume that only 0.045 out of 0.45 ppbv/fCi/SCM in the observed $\Delta O_3 / \Delta^7 Be$ ratio can be expected from the stratospheric contribution based on our PMF analysis, the tropospheric contribution to the observed O_3 variability is about 90% at Bermuda. This result is consistent with that by Li et al. [2002].

The NO_y-PAN factor reflects O_3 production within the troposphere. During the oxidation of CO and hydrocarbons, freshly emitted NO_x can be converted to HNO_3 and PAN, and O_3 is produced. The observed O_3 variation accounted for by this factor is about 30%, less than that by the ^{7}Be factor. There are only two main factors for PAN variability (Fig. 2). Beside the NO_y-PAN factor, the other one is the CH_4-halocarbon factor. The latter is the most dominant factor for CO and CH_4 variability. It also contributes largely to the variability of the industrial tracer C_2Cl_4, suggesting that this factor is associated with air masses affected by industrial emissions. There is not a significant PAN signal in the hydrocarbon factor, which has large CO, CH_4, and C_2Cl_4 signals because the seasonal trend of this factor is opposite to that of PAN. The lack of NO_y signal in the CH_4-halocarbon factor, despite its large PAN signal, may reflect the different seasonal trends of NO_y and PAN during TOPSE [Wang et al., 2003]. The sum of NO_y components including PAN and HNO_3 is generally higher than the observed NO_y and the former has a

stronger seasonal trend; the reason for this discrepancy is unclear [Wang et al., 2003]. A least-squares fit of PAN and NO_y shows that the variance of PAN explains about 30% of that of NO_y.

Figure 3 shows the 10-day backtrajectories for data points with high factor scores for the ^7Be and NO_y-PAN factors. Both are associated with the westerlies at northern mid latitudes in spring. The trajectories related to the ^7Be factor tend to extend further west into Europe whereas those related to the NO_y-PAN factor tend to cluster over the western Pacific. The backtrajectory altitude of the ^7Be factor resides mostly above 6 km, while those related to NO_y-PAN factor reside more likely at 2-6 km. Very few backtrajectories initiated at 0-2 km or south of 30° N. Mid-latitude emissions of O_3 precursors from East Asia, after being lifted out of the boundary layer, could have contributed significantly to the O_3 enhancement in the NO_y-PAN factor. Pollutions from the Middle East and southern Europe, lifted by convection to high altitudes (> 6 km), could also contribute to the enhancement.

The observed tropospheric O_3 increase at mid latitudes can now be attributed to different factors. We conduct the least-squares fits for the variability of observed O_3 and that explained by each factor (Fig. 4). We analyze the linear seasonal trend because it reasonably represents the increase of monthly median O_3 variation and facilitates the evaluation of the contribution from different factors. The observed seasonal O_3 increase is 5.4 ppbv/month while that from the contribution of all factors is 6.3 ppbv/month. The seasonal increase contributed by the NO_y-PAN factor is largest at 3.5 ppbv/month and that from the ^7Be factor is at 2.5 ppbv/month. Contributions from the other factors are

negligible. Photochemistry within the troposphere therefore appears to be more important to the seasonal O_3 increase than transport from the stratosphere.

3.2 High latitudes

At high latitudes, the ^{7}Be factor is still the largest contributor to the observed O_3 variability at about 35% (Fig. 5). The $\Delta O_3 / \Delta ^7$Be ratio in this factor is 0.03 fCi/SCM/ppbv (Fig. 6), lower than at mid latitudes. The lower ratio is entirely due to higher variability in ^{7}Be at high latitudes, which is consistent with higher ^{7}Be sources near the poles. The θ factor is the other one that has a large contribution (25%) of the observed O_3 variability. It also explains 60% and 20-30% of the variability in θ and many halocarbons, respectively. The NO_y-PAN factor, in contrast, accounts for only about 5% of the observed O_3 variability.

The 10-day backtrajectories for data points with high factor scores in the ^{7}Be and θ factors at high latitudes are quite different (Fig. 7). A large fraction of data contributing to the ^{7}Be factor circulated within the polar region north of 60° N. These backtrajectories reside generally above 6 km. In contrast, most of the data for the θ factor came from regions south of 60° N carried by the strong westerlies and were transported northward in the western United States. The related backtrajectories more likely reside below 6 km. Higher O_3 concentrations appear to be transported in the middle troposphere from the lower latitudes into high latitudes. Despite low in situ chemical production of O_3 [Wang et al., 2003], photochemical production of O_3 within the troposphere, through long-range transport from lower latitudes where photochemistry is active, still contributes significantly to the observed O_3 variability at high latitudes.

These two factors also account for much of the explained variability in θ. The gradient of θ is much stronger from the stratosphere into the troposphere as compared to that from mid to high latitudes in the troposphere [e.g., Holton, 1995]; the former is reflected in the vertical stability in the stratosphere and the latter is limited by tropospheric baroclinic adjustment processes. Similarly we find that the θ-CH_3Cl factor that explains most of the variability of θ at mid latitudes (Fig. 1) is related to transport from the subtropics into mid latitudes (not shown) and that it is associated with transport of CH_3Cl into the region. The larger contribution of latitudinal transport to the observed variability of θ across a much smaller gradient compared to transport from the stratosphere reflects much stronger latitudinal mixing in the northern hemisphere.

Although the ^7Be and θ factors account for about 60% of the observed O_3 variability at high latitudes, their contribution to the seasonal trend of tropospheric O_3 is much smaller (Fig. 8). The observed seasonal trend for tropospheric O_3 at high latitudes is 5.5 ppbv/month; the trend explained by all 7 factors is 4.6 ppbv/month. The ^7Be and θ factors account for 0.8 and 0.6 ppbv/month, respectively. The bulk of the seasonal O_3 increase is attributed to the NO_y-PAN and CH_4-halocarbon factors, accounting for 1.3 ppbv/month and 1.7 ppbv/month, respectively. These two factors also explain about 90% of the variability in observed PAN concentrations (Figs. 5 and 6). PAN is of tropospheric origin. These two factors therefore signify the effects of tropospheric production on the seasonal increase of tropospheric O_3.

The 10-day backtrajectories for data points with high factors scores in the NO_y-PAN factor (Fig. 7) show two primary pathways of transport via either mid-latitude westerlies over the Pacific or across the polar region. East Asia and northern Europe are

the likely source regions for the transported reactive nitrogen. Comparing to the transport of reactive nitrogen at mid latitudes (Fig. 3), the transport into the high latitudes tends to occur more below 6 km and is more likely to be affected by surface emissions.

Air masses contributing to the CH_4-halocarbon factor tend to be more stagnant than those to the NO_y-PAN factor with a large fraction of air circulating over Canada in the last 10 days. The tracer profile of the CH_4-halocarbon factor also reflects the origins of air masses. Among the 7 factors, two account for about 80% of the observed CH_4 variability. One is the CH_4-halocarbon factor. The other factor, which accounts for about 35% of the observed CH_4 variability, is associated with the seasonal decrease of hydrocarbons as defined largely by C_2H_2 and C_3H_8 (Fig. 5). The strong CH_4 signal likely reflects natural gas leaks from Russia, which has a large reservoir and active production of natural gas [van Meurs & Associates, 1997].

The CH_4-halocarbon and θ factors have strong halocarbon signatures (Figs. 5 and 6). These two factors and the hydrocarbon factor explain most of the observed variability in these species. Production of CFC-11 and Halon-1211 has been banned in developed countries. The halocarbon signals in the cross-Pacific transport as illustrated by the θ factor likely reflect the release of these halocarbons from China. The halocarbon signals in the CH_4-halocarbon factor appear to suggest continuing release of halocarbons (including CFC-11 and Halon-1211) from Russia.

Our results on the stratospheric contribution to the O_3 variability and seasonal trend are generally consistent with those derived from the global 3-D simulation by Allen et al. [2003]. The two results cannot be compared directly because we can only examine the variability and trend using our methodology while Allen et al. could estimate the

stratospheric contribution to O_3 concentrations. Dibb et al. [2003], by analyzing the O_3-^{7}Be correlation, found that high-latitude O_3 from the stratosphere does not contribute to the seasonal O_3 increase; we draw a similar conclusion in our analysis. They estimated that >85% of high-latitude O_3 is related to the stratospheric source by further interpreting the "residual O_3" from the intercept values of O_3-^{7}Be least-squares fitting. This estimate is larger than our estimates, although we have attempted to resolve only the variability. Browell et al. [2003] suggests that > 80% of the O_3 trend is due to tropospheric photochemistry on the basis of O_3 correlations with observed aerosol concentrations and model computed potential vorticity. Our result at high latitudes agrees well with their estimate. At mid latitudes, we estimate a much higher stratospheric contribution (about 40%) to the observed O_3 trend. It is unclear if their estimate would be closer to ours if only observations at middle latitude (rather than the whole dataset) are considered in their analysis.

4. Conclusions

PMF and PCA analysis techniques are applied to analyze the TOPSE observations to investigate the various factors contributing to the observed variability of tropospheric O_3 and its seasonal trend observed during spring 2000 at mid and high latitudes. A suite of 14 chemical tracers and 1 dynamic tracer were used to define the chemical characteristics of the air masses. The coincident data of 15 tracers we used in the analysis are a small subset of all TOPSE measurements due largely to the availability of ^{7}Be measurements. As a result, our results are biased towards the middle and upper troposphere. We find no bias in the probability distribution of O_3 concentrations (binned by 10 ppbv) in the subset, but a larger fraction of measurements, 70% vs. 50% for the

whole dataset, was taken at 5-8 km. The seasonal O_3 trend in the subset is in agreement with all O_3 data above 5 km.

We find that the PMF results are clearer for physical interpretation than those of PCA. Computed 10-day backtrajectories contributing to each factor are examined to define the geographical characteristics of the air masses. The chemical characteristics from factor analysis and the associated backtrajectories provide complimentary information that is in general consistent with our current understanding of the source distributions of chemical and dynamical tracers. While it cannot offer the depth of information that can be extracted from 3-D model simulations, the analysis provides important observation-based constraints on the controlling factors for springtime O_3 variability and its seasonal trend at northern mid and high latitudes.

The intercontinental nature of pollution transport in spring is clearly evident in our results. At mid latitudes, the timescale of transport of pollutants from Eurasia to North America is only 1-2 weeks by mid-latitude westerlies. Coupled with a favorable photochemical environment, O_3 production by reactive nitrogen emitted from Eurasia (with possible contributions from North America) is a major factor leading to the observed O_3 variability and seasonal trend during TOPSE. We estimate that this source, related to the PAN-NO_y factor, explains an O_3 enhancement of 11 ppbv and a seasonal trend of 3.5 ppbv/month.

At high latitudes, the effect of intercontinental transport becomes even more prominent in part because springtime photochemistry in the region is relatively slow. It is manifested in the transport of O_3 and its precursors. The dominant tropospheric factor affecting the observed O_3 variability is related to the transport of potential temperature (θ

factor) from lower latitudes, where the high availability of photons and anthropogenic emissions result in a general "background" O_3 enhancement compared to high latitudes. We estimate that it contributes to an O_3 enhancement of about 11 ppbv but only 0.6 ppbv/month in the seasonal trend. In contrast, the PAN-NO_y and CH_4-halocarbon factors, which explain all the variability of PAN (120 and 60 pptv, respectively), contribute respectively 1.3 and 1.7 ppbv/month to the seasonal trend even though their contribution to the O_3 variability is about 4 ppbv each. Therefore, transport of O_3 from lower latitudes, which is poor in reactive nitrogen, tends to dominate O_3 variability while transport of reactive nitrogen rich air masses tends to dominate the seasonal trend. Cross-Pacific transport is important in all cases; cross-Arctic transport is also important for reactive nitrogen rich air masses. In addition, the halocarbon signals in the CH_4-halocarbon factor appear to indicate continuing release of halocarbons (including CFC-11 and Halon-1211) from Russia.

Transport from the stratosphere, diagnosed through the ^{7}Be factor, is also important. It is manifested mostly above 6 km while transport of tropospheric O_3 and its precursors is more likely to be important at 2-6 km, indicating that the stratospheric influence decreases with altitude. We estimate that it contributes to an O_3 enhancement of about 14 ppbv (35-40%) for data with O_3 concentrations < 100 ppbv at mid and high latitudes. There is a large latitudinal difference in its contribution to the seasonal trend, at 2.5 ppbv/month (40%) at mid latitudes but only 0.8 ppbv/month (<20%) at high latitudes. The difference probably reflects increasing activity of the more vigorous dynamical systems at mid latitudes in spring.

Acknowledgement

This work is supported by funding from the National Science Foundation and the NASA ACMAP program. We thank P. K. Hopke for his help in the early stage of the project.

References

Allen, D., et al., An estimate of the stratospheric contribution to springtime tropospheric ozone maxima using TOPSE measurements and beryllium-7 simulations, *J. Geophys. Res., 108*, 8355, doi:10.1029/2001JD001428, 2003.

Atlas, E. L., B. A. Ridley, and C. Cantrell, The Tropospheric Ozone Production about the Spring Equinox (TOPSE) Experiment: Introduction, *J. Geophys. Res., 108*, 8353, doi:10.1029/2002JD003172, 2003.

Berntsen, T. K., S. Karlsdottir, and D.A. Jaffe, Influence of Asian emissions on the composition of air reaching the northwestern United States, *Geophys. Res. Lett, 26,* 2171-2174, 1999.

Bey I., D. J. Jacob, J. A. Logan, R. M. Yantosca, Asian chemical outflow to the Pacific: origins, pathways and budgets, *J. Geophys. Res., 106,* 23,097-23,114, 2001.

Blake, N. J., D. R. Blake, B. C. Sive, A. S. Katzenstein, S. Meinardi, O. W. Wingenter, E. L. Atlas, F. Flocke, B. A. Ridley, and F. S. Rowland, The seasonal evolution of NMHCs and light alkyl nitrates at middle to high northern latitudes during TOPSE, *J. Geophys. Res., 108,* 8359, doi:10.1029/2001JD001467, 2003.

Browell, E. et al., Ozone, aerosol, potential vorticity, and trace gas trends observed at high latitudes from February to May 200, *J. Geophys. Res.*, *108*, 8369, doi:10.1029/2001JD001390, 2003.

Cantrell, C., et al. Steady state free radical budgets and ozone photochemistry during TOPSE, *J. Geophys. Res.*, *108*, 8361, doi:10.1029/2002JD002198, 2003.

Carpenter, L. J., et al., Oxidized nitrogen and ozone production efficiencies in the springtime free troposphere over the Alps, *J. Gephys. Res., 105,* 14,547-14,559, 2000.

Draxler, R. R. and G. D. Hess, An Overview of the Hysplit 4 Modeling System for Trajectories, Dispersion, and Deposition, *Aust. Met. Mag., 47,* 295-308, 1998.

Dibb J. E., D. Meeker, R. C. Finkel, J. R. Southon, M. W. Caffee, and L. A. Barrie, Estimation of stratospheric input to the Arctic troposphere: ^{7}Be and ^{10}Be in aerosols at Alert, Canada, *J. Geophys. Res., 99,* 12855-12864, 1994.

Dibb, J. E. et al., Stratospheric influence on the northern North American free troposphere during TOPSE: ^{7}Be as a stratospheric tracer, *J. Geophys. Res., 108,* 8363, doi:10.1029/2001JD001347, 2003.

Holton, J. R., P. H. Haynes, M. E. McIntyre, A. R. Douglass, R. B. Rood, and L. Pfister, Stratosphere-troposphere exchange, *Rev. of Geophys., 33,* 403-439, 1995.

Jacob, D. J., J. A. Logan, and P. P. Murti, Effect of rising Asian emissions on surface ozone in the United States, *Geophys. Res. Lett., 26,* 2175–2178, 1999.

Jaffe, D., et al., Transport of Asian air pollution to North America, *Geophys. Res. Lett., 26,* 711-714, 1999.

Lee, E., C. K. Chan, and P. Paatero, Application of positive matrix factorization in source apportionment of particulate pollutants in Hong Kong. *Atmos. Envron*., *33*, 3201-3212, 1999.

Lee-Taylor, J. M. Brasseur, G. P., and Y. Yokouchi, A preliminary three-dimensional global model study of atmospheric methyl chloride distributions, *J. Geophys.Res.,106*, 34221-34233, 2001

Levy, H., II, J.D. Mahlman, W.J. Moxim, and S.C. Liu, Tropospheric ozone: The role of transport, *J. Geophys. Res., 88,* 3753-3772, 1985.

Li, Q., et al., Stratospheric versus pollution influences on ozone at Bermuda: Reconciling past analyses, *J. Geophys. Res., 107*, 4611, doi:10.1029/2002JD002138, 2002.

Liu, H., D. J. Jacob, I. Bey, and R. M. Yantosca, Constraints from ^{210}Pb and ^{7}Be on wet deposition and transport in a global three-dimensional chemical transport model, *J. Geophys. Res., 106,* 12,109-12,128, 2001.

Liu, S. C., M. Trainer, F.C. Fehsenfeld, D.D. Parrish, E. J. Williams, D.W. Fahey, G. Hubler, and P.C. Murphy, Ozone production in the rural troposphere and the implications for regional and global ozone distributions, *J. Geophys. Res., 92,* 10463-10482, 1987.

Logan, J. A., Tropospheric ozone: Seasonal behavior, trends, and anthropogenic influence, *J. Geophys. Res., 90,* 10463-10482, 1985.

Mauzerall, D. L., D. Narita, H. Akimoto, L. Horowitz, S. Walters, D. Hauglustaine, G. Brasseur, Seasonal characteristics of tropospheric ozone production and mixing ratios over East Asia: A global three-dimensional chemical transport model analysis, *J. Geophys. Res.*, *105*, 17895-17910, 2000.

Kaiser, H. P., The varimax criterion for analytical rotation in factor analysis, *Psychometrika, 23*, 187-196, 1958.

Kanamitsu, M., Description of the NMC Global Data Assimilation and Forecast System, *Weather and Forecasting, 4,* 335-342, 1989.

Otlmans, S. J., and H. Levy, II., Seasonal cycle of surface ozone over the western North Atlantic, *Nature, 358,* 392-394, 1992.

Paatero, P., Least squares formulation of robust non-negative factor analysis, *Chemometrics and Intelligent Laboratory Systems,* 37, 23-35, 1997.

Paatero, P., P. K. Hopke, X.-H. Song and Z. Ramadan, Understanding and controlling rotations in factor analytic models. *Chemometrics and Intelligent Laboratory Systems*, *60*, 253 – 264, 2002.

Paterson, K.G., J.L. Sagady, and D.L. Hooper, Analysis of air quality data using positive matrix factorization, *Environ. Sci. Technol*, *33*, 635-641, 1999.

Penkett, S.A., and K.A. Brice, The spring maximum in photo-oxidants in the Northern Hemisphere troposphere, *Nature, 319,* 655-657, 1986.

Pochanart, P., H. Akimoto, S. Maksyutov, and J. Staehelin, Surface ozone at the Swiss Alpine site Arosa: The hemispheric background and the influence of large-scale anthropogenic emissions, *Atmos. Environ., 35,* 5553-5566, 2001.

Polissar, A. V., P. K. Hopke, P. Paatero, W. C. Malm, and J. F. Sisler, Atmospheric aerosol over Alaska, 2. Elemental composition and sources, *J. Geophys. Res., 103,* 19,045 – 19,057, 1998.

Press, W. H., S. A. Teukolsky, W. T. Vetterling, and B. F. Flannery, *Numerical Recipes in Fortran*, Cambridge University Press, 963 pp., 1992.

Ramadan, Z., X.-H. Song, and P. K. Hopke, Identification of source of Phoenix aerosol by positive matrix factorization, *J. Air & Waste Mange. Assoc*., *50*, 1308 – 1320, 2000.

Stohl, A., Computation, accuracy and applications of trajectories - A review and bibliography, *Atmos. Environ., 32,* 947-966, 1998.

Tanimoto, H, et al., Seasonal cycles of ozone and oxidized nitrogen species in northeast Asia 2. A model analysis of the roles of chemistry and transport, *J. Geophys. Res., 107,* 4706, doi:10.1029/2001JD001497, 1997.

Wang, Y., D. J. Jacob, and J. A. Logan, Global simulation of tropospheric O_3-NO_x-hydrocarbon chemistry, 3. Origin of tropospheric ozone and effects of non-methane hydrocarbons, *J. Geophys. Res., 103,* 10,757-10,768, 1998.

Wang, Y., et al., Springtime photochemistry at northern mid and high latitudes, *J. Geophys. Res.*, *108*, 8358, doi:10.1029/2002JD002227, 2003.

Wild, O., and H. Akimoto, Intercontinental transport of ozone and its precursors in a three-dimensional global CTM, *J. Geophys. Res., 106,* 27,729-27,744, 2001.

van Meurs & Associates**,** *World Fiscal Systems for Gas – 1997*, Volume I, New York, 1997.

Yokouchi, Y., et al., A strong source of methyl chloride to the atmosphere from tropical coastal land, *Nature, 403,* 295-298, 2000.

Zanis, P., P. S. Monks, E. Schuepbach, and S. A. Penkett, The role of in situ photochemistry in the control of ozone during spring at the Jungfraujoch (3580 m asl): Comparison of model results with measurements, *J. Atmos. Chem., 37,* 1-27, 2000.

Figure captions

Fig. 1. Explained variation (defined in section 2) of each tracer in the 7 factors at mid latitudes (40-60° N). The last panel in the right column shows the EV percentages explained by all the factors. The factors are named after the tracers that have strong signals. The results are for data with O_3 concentrations < 100 ppbv.

Fig. 2. The tracer variation ([tracer]-[tracer]$_{min}$) explained by each factor. The results are for data with O_3 concentrations < 100 ppbv.

Fig. 3. 10-day backtrajectories of data points that rank top 30% by the factor score (Eq. 2) for the NO_y-PAN and ^{7}Be factors at mid latitudes. The pluses show the locations of measurements. The backtrajectory location every hour is represented by a dot and the end point is marked by a diamond. The results are for data with O_3 concentrations < 100 ppbv.

Fig. 4. Least-squares fits of O_3 variation ([O_3]-[O_3]$_{min}$) as a function of Julian day for the observed and PMF fitted O_3, and that explained by each factor at mid latitudes. The monthly medians for the O_3 variations from the observations and the sum of all factors are also shown. The minimum O_3 concentration in the dataset is 27 ppbv. The results are for data with O_3 concentrations < 100 ppbv.

Fig. 5. Same as Fig. 1 but for high latitudes (60-85 ° N).

Fig. 6. Same as Fig. 2 but for high latitudes.

Fig. 7. Same as Fig. 3 but for the ^{7}Be, θ, NO_y-PAN, and CH_4-halocarbon factors at high latitudes.

Fig. 8. Same as Fig. 4 but for high latitudes. The minimum O_3 concentration in the dataset is 26 ppbv.

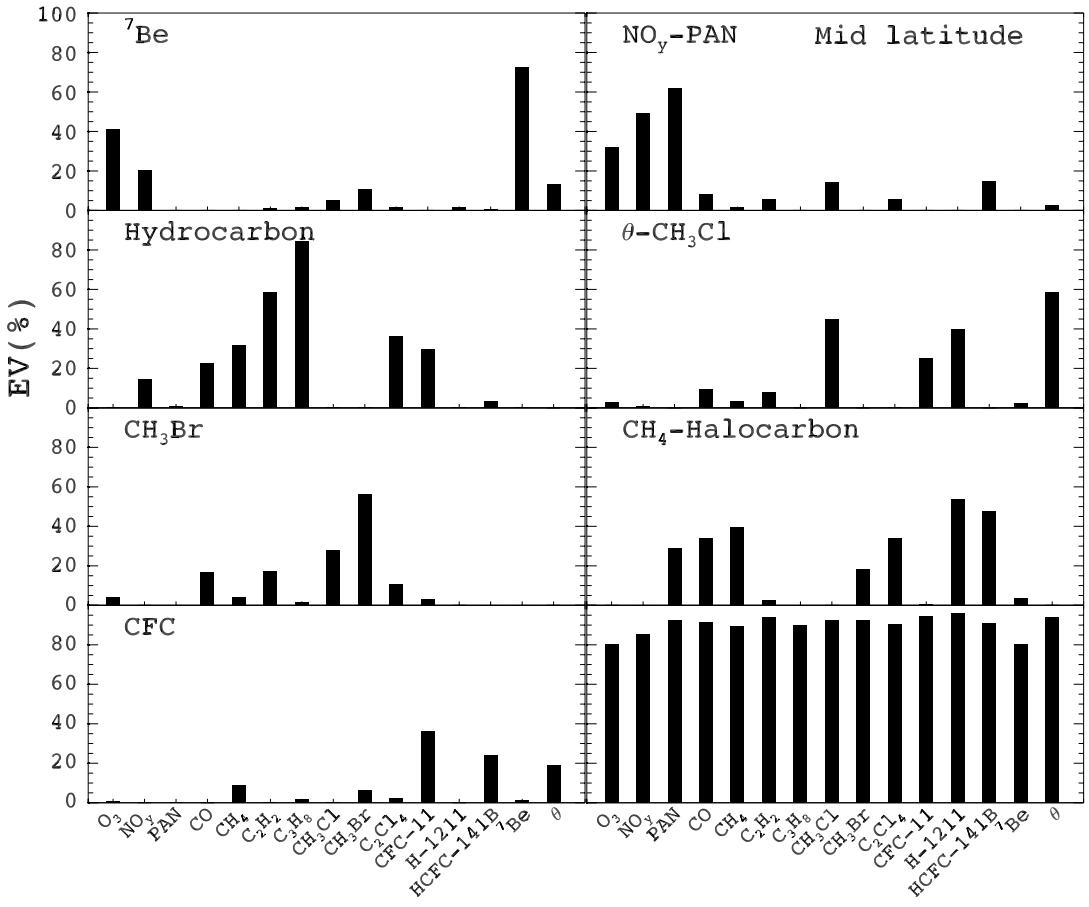
EV(%)
^{7}Be
NO_y-PAN
Mid latitude
Hydrocarbon
θ-CH_3Cl
CH_3Br
CH_4-Halocarbon
CFC
O_3
NO_y
PAN
CO
CH_4
C_2H_2
C_3H_8
CH_3Cl
CH_3Br
C_2Cl_4
CFC-11
H-1211
HCFC-141B
^{7}Be
θ

Figure 1

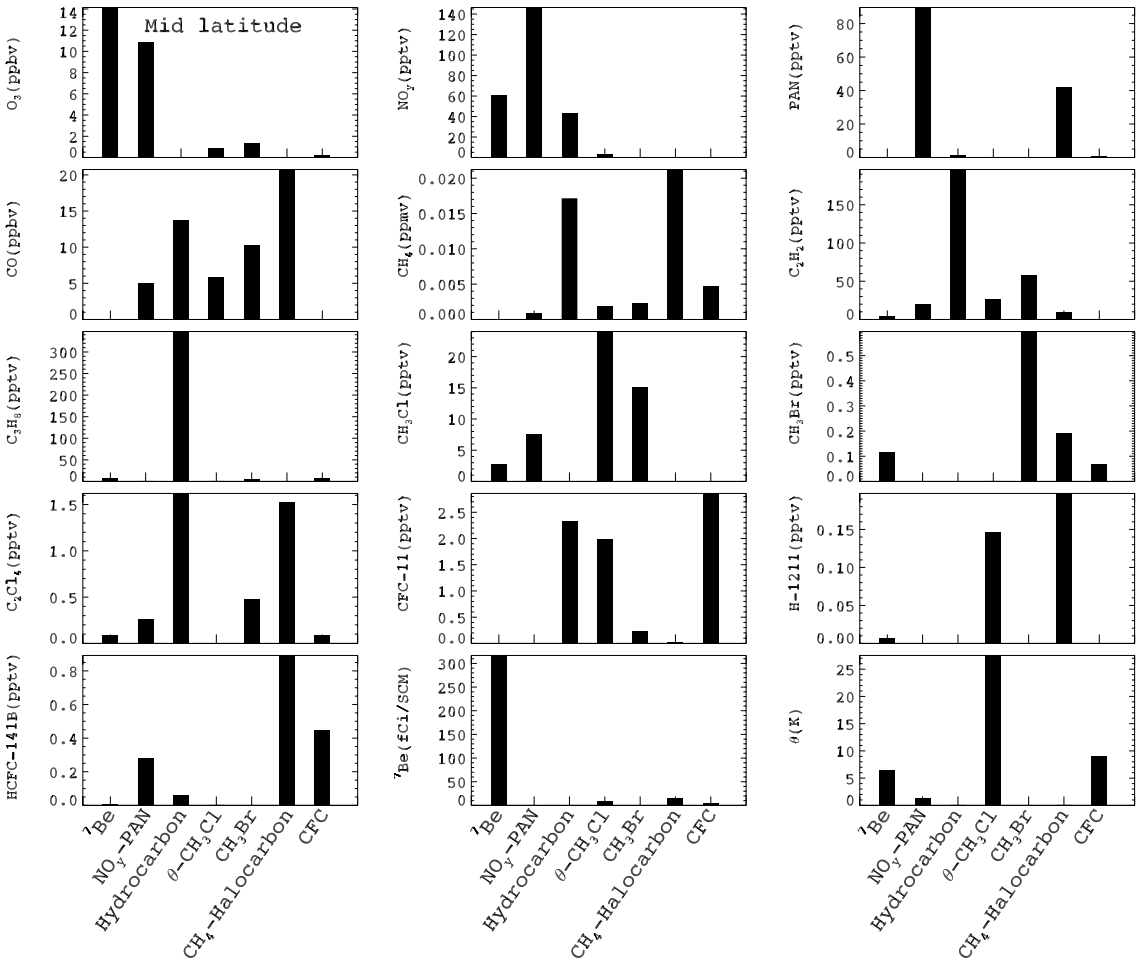
Mid latitude
O3(ppbv)
NOy(pptv)
PAN(pptv)
CO(ppbv)
CH4(ppmv)
C2H2(pptv)
C2H6(pptv)
CH3Cl(pptv)
CH3Br(pptv)
C2Cl4(pptv)
CFC-11(pptv)
H-1211(pptv)
HCFC-141B(pptv)
7Be(fCi/SCM)
θ(K)
7Be
NOy-PAN
Hydrocarbon
θ-CH3Cl
CH3Br
CH4-Halocarbon
CFC

Figure 2

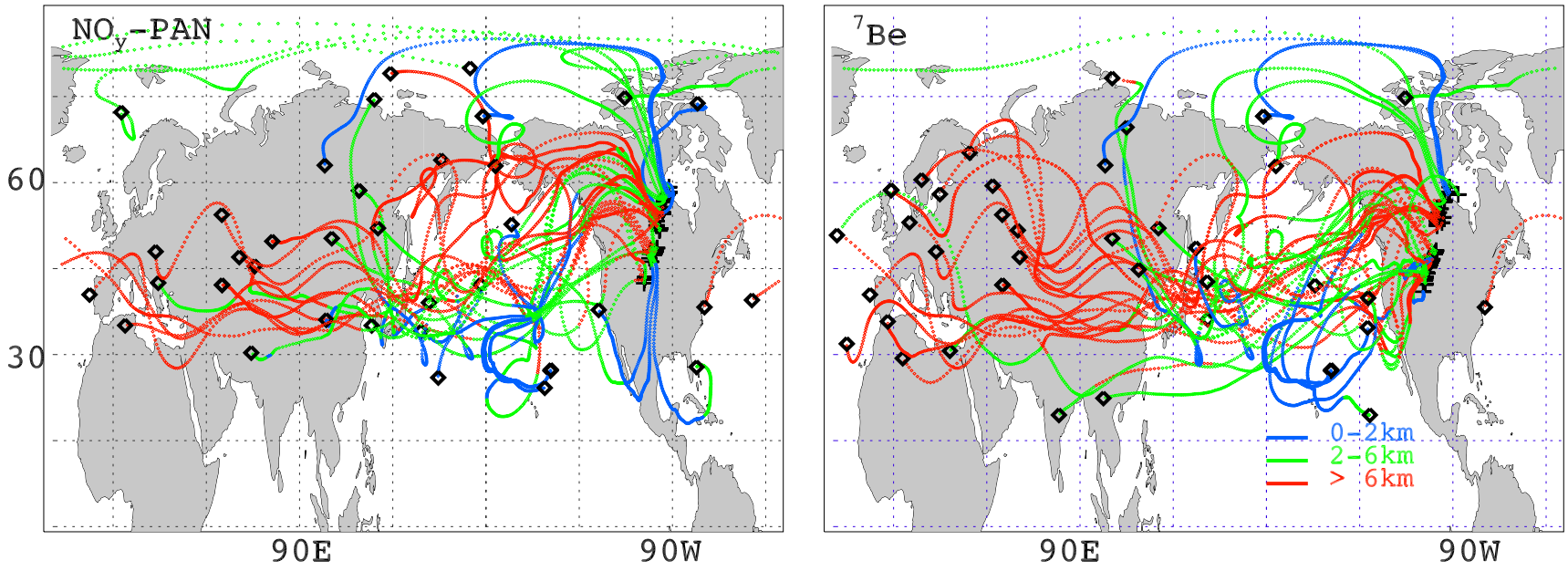

Figure 3

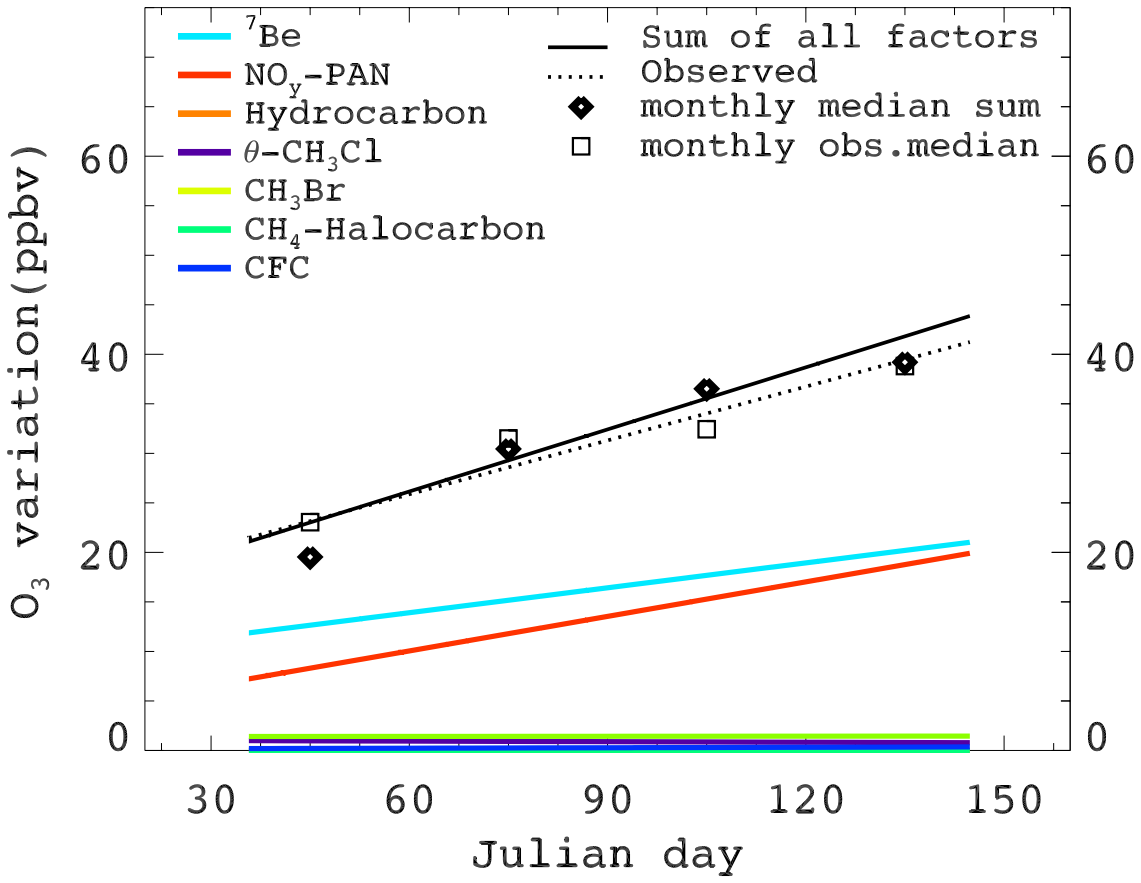
^{7}Be
NO_y-PAN
Hydrocarbon
θ-CH_3Cl
CH_3Br
CH_4-Halocarbon
CFC
Sum of all factors
Observed
monthly median sum
monthly obs.median
O_3 variation(ppbv)
0
20
40
60
30
60
90
120
150
Julian day

Figure 4

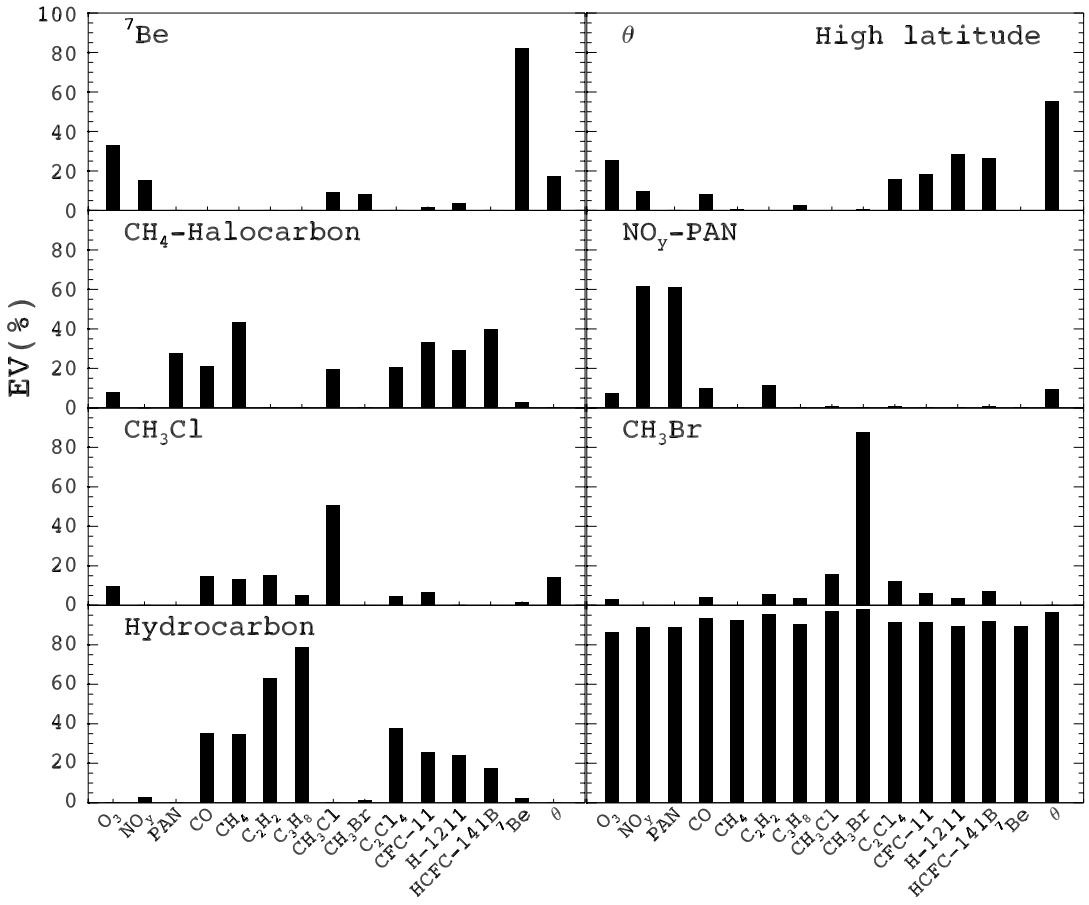
EV(%)
^{7}Be
θ
High latitude
CH_4-Halocarbon
NO_y-PAN
CH_3Cl
CH_3Br
Hydrocarbon
O_3
NO_y
PAN
CO
CH_4
C_2H_2
C_3H_8
CH_3Cl
CH_3Br
C_2Cl_4
CFC-11
H-1211
HCFC-141B
^{7}Be
θ

Figure 5

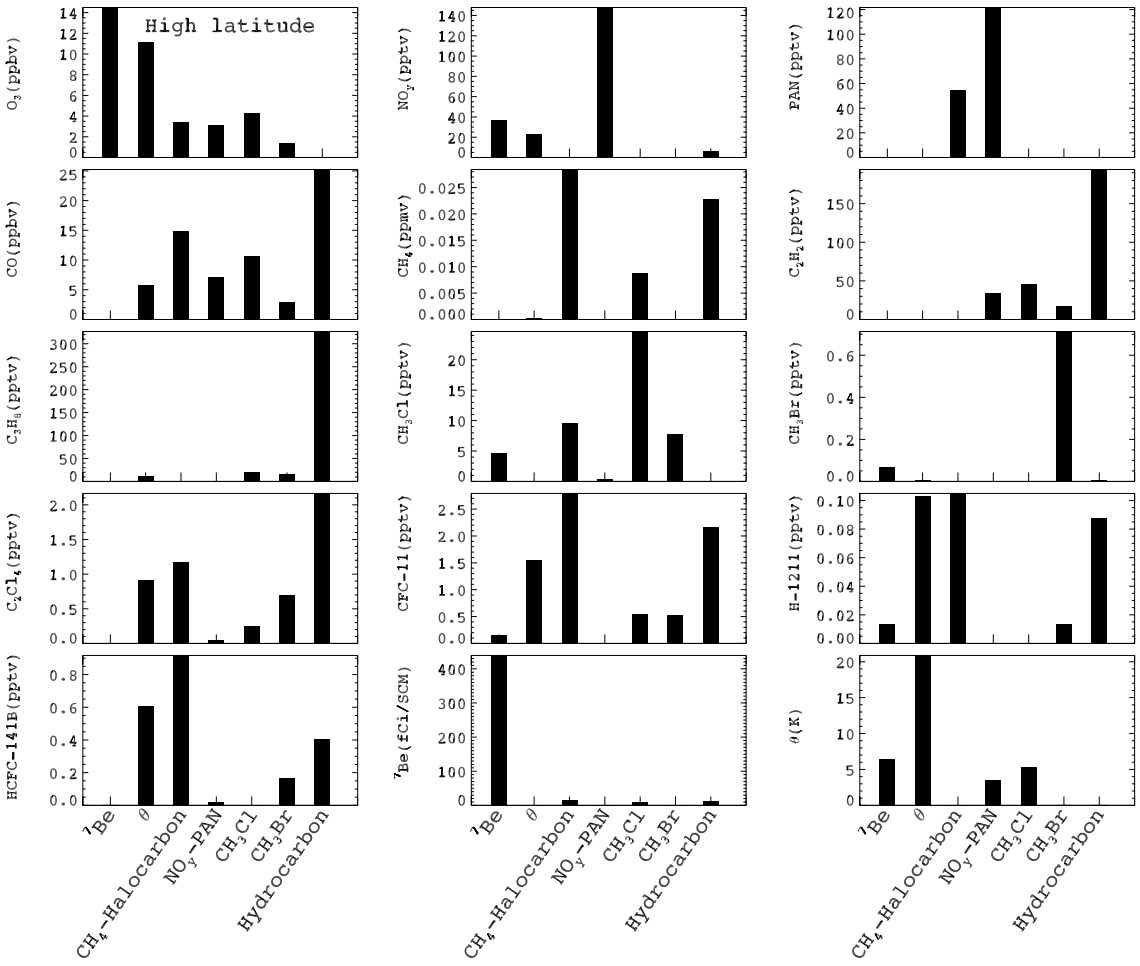
High latitude
O3(ppbv)
NOy(pptv)
PAN(pptv)
CO(ppbv)
CH4(ppmv)
C2H2(pptv)
C2H6(pptv)
CH3Cl(pptv)
CH3Br(pptv)
C2Cl4(pptv)
CFC-11(pptv)
H-1211(pptv)
HCFC-141B(pptv)
7Be(fCi/SCM)
θ(K)
7Be
θ
CH4-Halocarbon
NOy-PAN
CH3Cl
CH3Br
Hydrocarbon

Figure 6

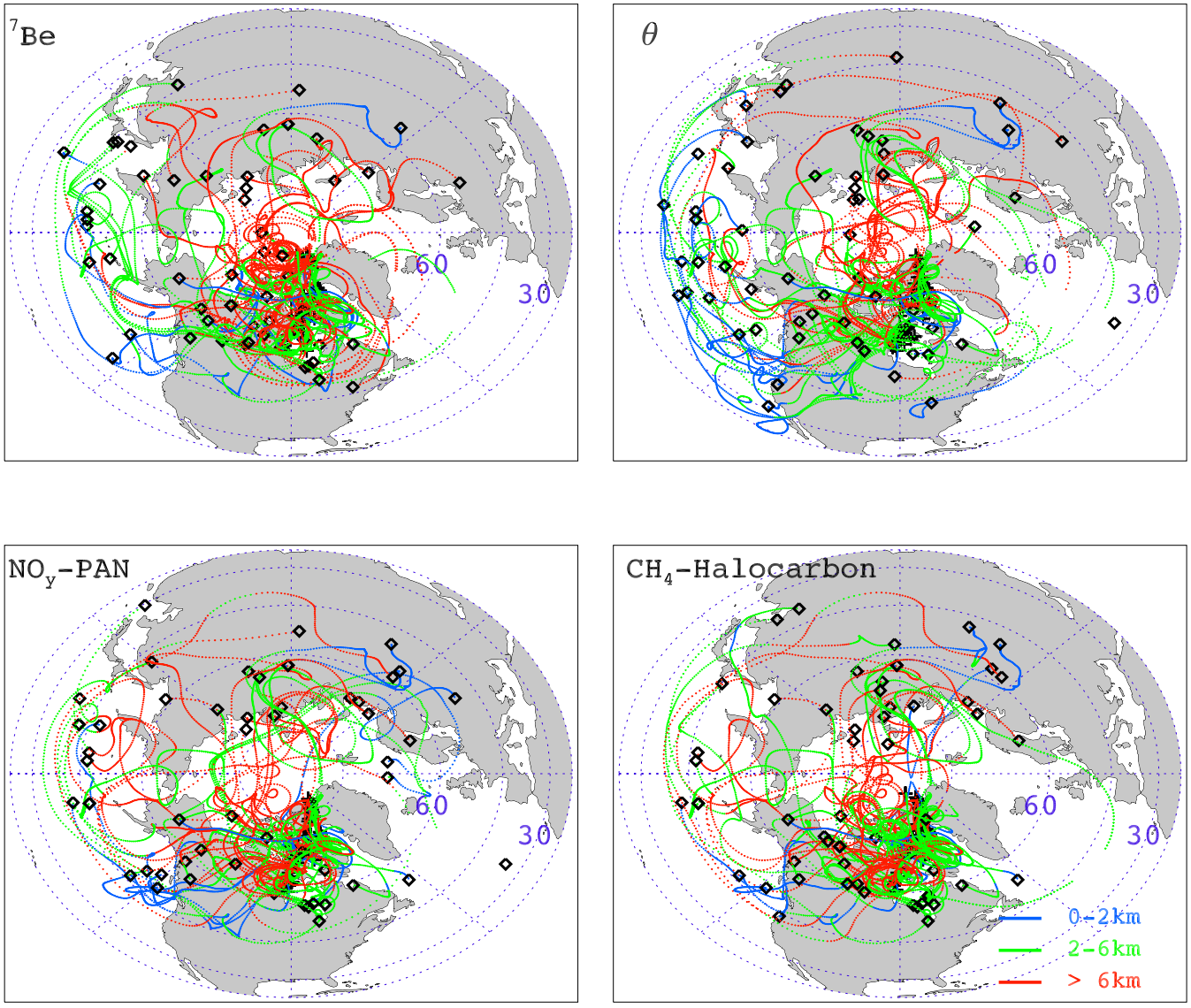
^{7}Be
θ
NO_y-PAN
CH_4-Halocarbon
60
30
60
30
60
30
60
30
0-2km
2-6km
> 6km

Figure 7

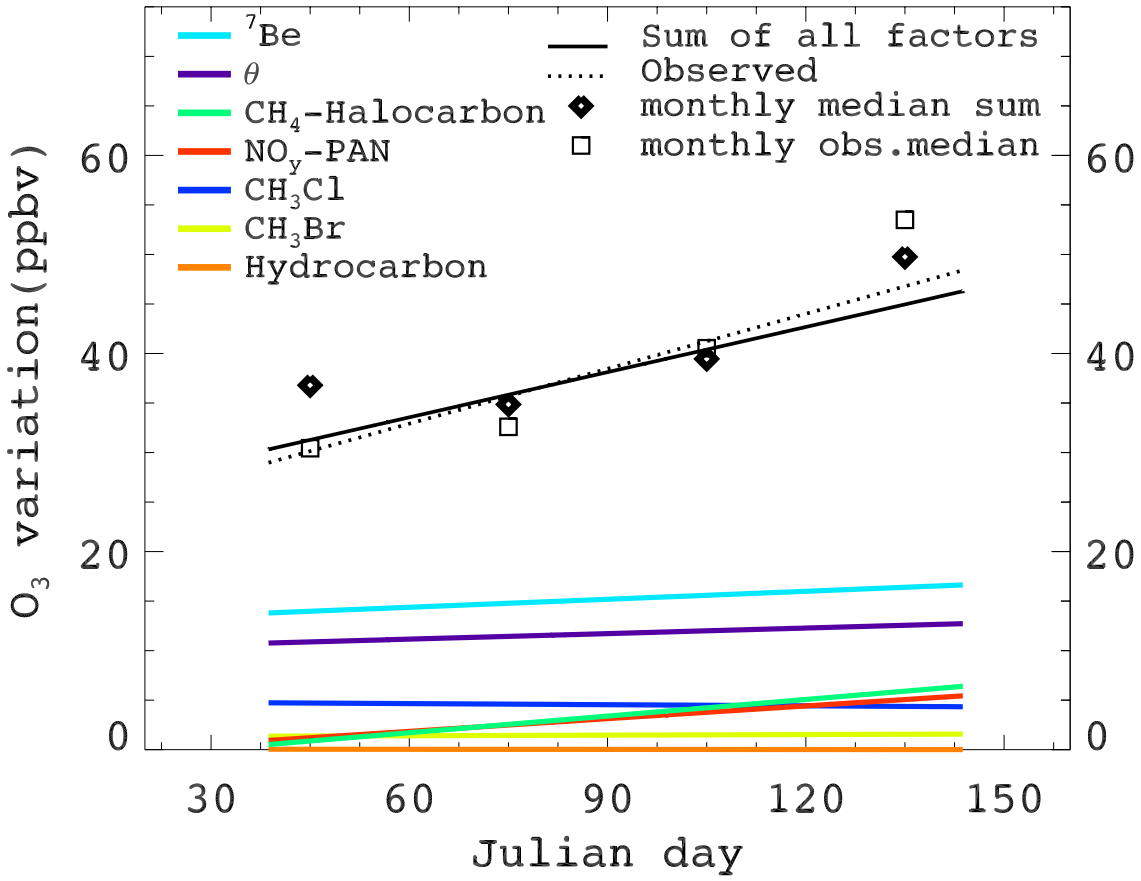
^{7}Be
θ
CH_4-Halocarbon
NO_y-PAN
CH_3Cl
CH_3Br
Hydrocarbon
Sum of all factors
Observed
monthly median sum
monthly obs.median
O_3 variation(ppbv)
0
20
40
60
30
60
90
120
150
Julian day

Figure 8